A Hybrid Explicit-Implicit Numerical Algorithm for the Three-Dimensional Compressible Navier-Stokes Equations

Doyle D. Knight*
Rutgers University, New Brunswick, New Jersey

A hybrid explicit-implicit numerical algorithm has been developed for the three-dimensional mean compressible Navier-Stokes equations. The algorithm combines the explicit finite difference algorithm of MacCormack and an implicit algorithm for the viscous sublayer and transition wall regions of the turbulent boundary layers. The algebraic turbulent eddy-viscosity model of Baldwin and Lomax is employed. A body-oriented coordinate transformation is utilized to facilitate treatment of arbitrary flow regions. The hybrid algorithm has been vectorized on the CDC CYBER 203 computer using the SL/1 vector programming language developed at NASA Langley. The accuracy of the numerical algorithm, established previously for two-dimensional flows with strong viscous-inviscid interaction (including flow separation), is validated for three-dimensional flows. The algorithm is applied to the interaction of an oblique shock wave with a turbulent boundary layer in three dimensions. The computed results generally are found to be in close agreement with the experimental data. The hybrid algorithm is shown to provide a substantial improvement in computational efficiency compared to a vectorized MacCormack explicit algorithm alone.

Introduction

THE understanding of three-dimensional shock wave/turbulent boundary-layer interactions (denoted as "3-D turbulent interactions") is an important problem in high-speed fluid mechanics. The phenomenon is manifested in a wide variety of practical applications, including internal flows (e.g., high-speed aircraft inlets and transonic compressors), high-speed aerodynamics (e.g., in the vicinity of the juncture of aircraft or missile fuselage and wings or control surfaces), and gas dynamic lasers.

Although a complete physical understanding of 3-D turbulent interactions is lacking, substantial progress has been achieved in recent years. A brief sampling of recent experimental investigations of 3-D turbulent interactions includes the studies of Law,[1] Freeman and Korkegi,[2] Oskam et al.,[3,4] Peake,[5] Settles et al.,[6] and Dolling et al.[7] In addition, scaling laws for 3-D turbulent interactions recently have been proposed by Settles and Bogdonoff[8] for 2-D and 3-D compression corners, and by Dolling and Bogdonoff[9] for sharp fin-induced 3-D turbulent interactions. A brief sampling of recent theoretical investigations of flowfields exhibiting 3-D turbulent interactions includes the studies of supersonic turbulent corner flows by Hung and MacCormack,[10] Shang et al.,[11] and Horstman and Hung.[12] In addition, Hung and Chaussee[13] computed supersonic turbulent flow past an inclined ogive-cylinder flare, and Hung[14] treated the impingement of an oblique shock wave on a cylinder.

The focus of the present work is the development and application of an efficient hybrid numerical algorithm for the computation of high-speed flows exhibiting 3-D turbulent interactions. The mean compressible 3-D Navier-Stokes equations are employed, together with the algebraic turbulent eddy-viscosity model of Baldwin and Lomax.[15] A body-oriented coordination transformation is utilized to facilitate treatment of arbitrary flow regions. The algorithm combines the explicit finite difference method of MacCormack et al.[16,17] and an implicit algorithm for the viscous sublayer and transition wall regions of the turbulent boundary layers. The algorithm represents the extension to three-dimensional flows of the technique developed previously by the author for the two-dimensional compressible Navier-Stokes equations.[18-20] The present numerical code is written in the SL/1 vector programming language developed at NASA Langley Research Center, and is executed on the CYBER 203 vector-processing computer at NASA Langley. In the following sections the details of the numerical algorithm are presented. The accuracy of the method is validated by consideration of the case of supersonic turbulent flow in a 90-deg corner. The algorithm is applied to the interaction of an oblique shock wave with a turbulent boundary layer in three dimensions, and the results compared with experimental data.

Received Nov. 10, 1982; presented as Paper 83-0223 at the AIAA 21st Aerospace Sciences Meeting, Reno, Nev., Jan. 10-13, 1983; revision submitted Oct. 6, 1983.

*Associate Professor, Department of Mechanical and Aerospace Engineering. Member AIAA.

Method of Solution

Coordinate Transformation

A set of surface-oriented curvilinear coordinates, denoted by $\xi(x,y,z)$, $\eta(x,y,z)$, and $\zeta(x,y,z)$, are introduced in order to facilitate treatment of arbitrary flow regions. The concept is illustrated in Fig. 1 for the particular configuration of flow into a corner formed by a wedge attached to a flat plate, which, in general, represents the cases considered in the present paper. The computational domain is denoted by the dotted lines. The upstream and downstream planes ABHG and EDJK, respectively, are mapped into the unit square in the $\xi=0$ and 1 planes (Fig. 2). The surface ABCDEF, coinciding with the flat plate, is mapped into the unit square in the $\zeta=0$ planes, while the upper surface GHIJKL maps into the unit square in the $\zeta=1$ plane. The left boundary surface AFEKLG, including the wedge surface, is mapped into the unit square in the $\eta=0$ plane, while the right boundary surface BCDJIH maps into the corresponding location in the $\eta=1$ plane. The curvilinear coordinates may be obtained by a variety of techniques.[21] For the results presented herein, however, the simplified nature of the flow geometry allowed the coordinates to be constructed algebraically in the physical domain using simple geometric stretching.

The coordinate transformation maps a nonuniform grid of mesh points in the physical domain which is capable of resolving the significant features of the flow into a uniform

rectilinear grid of points in the transformed domain with constant mesh spacing $\Delta\xi$, $\Delta\eta$, and $\Delta\zeta$. The Navier-Stokes equations are solved in the transformed domain, where the simple cubic domain and constant mesh spacing facilitate the application of the numerical algorithm. The flowfield in the physical domain is obtained through knowledge of the inverse transformation $x(\xi, \eta, \zeta)$, $y(\xi, \eta, \zeta)$, and $z(\xi, \eta, \zeta)$.

Governing Equations and Boundary Conditions

The governing equations are the full mean compressible Navier-Stokes equations in three dimensions using mass-averaged variables[22] and strong conservation form.[23] The molecular dynamic viscosity μ is given by Sutherland's law. The molecular Prandtl number Pr is 0.73 (air) and the turbulent Prandtl number Pr_t is 0.9.

The turbulent eddy viscosity ϵ is the two-layer model of Baldwin and Lomax[15] with additional modifications to treat the corner region formed by the wedge and flat plate. Within the inner layer, the eddy viscosity is

$$\epsilon_i = \rho(\kappa \ell D)^2 \omega \tag{1}$$

where ρ is the density and κ is von Kármán's constant. The length scale ℓ is Buleev's mixing length.[24] For an open corner formed by the normal intersection of two planes,[10,11,25]

$$\ell = \frac{2\tilde{y}\tilde{z}}{\tilde{y}+\tilde{z}+(\tilde{y}^2+\tilde{z}^2)^{1/2}} \tag{2}$$

where $\tilde{y}$ and $\tilde{z}$ are Cartesian coordinates as shown in Fig. 1. The Van Driest damping factor is $D = 1-\exp(-\ell u_*/26\nu_w)$, where $u_* = (|\tau_w|/\rho_w)^{1/2}$, τ_w is the wall shear stress, and ν_w the wall kinematic eddy viscosity. The quantity ω is the absolute value of the vorticity. The outer eddy viscosity is given by

$$\epsilon_o = \rho k C_{cp} F_{wake} F_{Kleb} \tag{3}$$

where $k = 0.0168$ and $C_{cp} = 2.08$. The value of C_{cp} is 30% above the value given by Baldwin and Lomax as discussed in Ref. 26. The function $F_{wake} = \ell_{max} F_{max}$, where $F_{max} = \max(\ell\omega D)$ and ℓ_{max} is the value of ℓ where $\ell\omega D$ is a maximum. For equilibrium boundary layers,[15] the function $\ell\omega D$ typically displays a single peak. For more complex flows involving strong viscous-inviscid interaction,[26-28] $\ell\omega D$ may display two peaks within the boundary layer. Since the outer eddy-viscosity formulation is intended to provide a velocity scale F_{max} and length scale ℓ_{max} representative of the outer region of the boundary layer, the outer peak in $\ell\omega D$ is chosen.[26,27] This modified form of the outer eddy-viscosity formulation was investigated only for a limited number of 2-D and 3-D turbulent interactions[26,27] at Mach 3, and as such represents an incomplete extension to the original Baldwin-Lomax model. Nevertheless, for the present paper, the determination of ℓ_{max} and F_{max} by the modified method differed from the original Baldwin-Lomax model only for $\alpha_g > 0$ (Fig. 1), and only on the boundary layer on the flat plate for $z_g < 2\delta_\infty$, where z_g is the distance from the wedge surface (Fig. 1). The Klebanoff intermittency correction is given by

$$F_{Kleb} = \left\{1 + 5.5\left(\frac{C_{Kleb}\ell}{\ell_{max}}\right)^6\right\}^{-1} \tag{4}$$

where $C_{Kleb} = 0.3$.

The turbulent eddy viscosity is implemented[10] by dividing the y-z plane into two regions (Fig. 3). In region I, the inner and outer eddy-viscosity profiles are obtained along $y = \text{const}$ lines, and the eddy viscosity is switched from the inner to the outer form at the location where $\epsilon_i > \epsilon_o$. In region II, the same approach is employed on $z = \text{const}$ lines.

The boundary conditions for the class of corner flows shown in Fig. 1 can be divided into five categories. First, on the upstream boundary ABGH ($\xi = 0$) the flow variables are held at freestream conditions or at conditions corresponding to a developed flat-plate boundary layer, depending on whether the flat-plate leading edge lies downstream or upstream, respectively, of the $\xi = 0$ plane. Second, on the downstream boundary EDJK ($\xi = 1$), the conventional zero gradient condition $\partial/\partial\xi = 0$ is applied. Third, on the solid boundaries corresponding to the flat plate and wedge surface, the velocity vector is set equal to zero, the temperature or adiabatic wall condition is specified, and the normal gradient of the pressure is set to zero.[18] Fourth, on the plane of symmetry AFLG, the normal component of the velocity is set to zero and the normal derivative of the remaining flow variables is set to zero. Finally, on the outer boundaries $\eta = 1$ and $\zeta = 1$, the zero gradient conditions $\partial/\partial\eta = 0$ and $\partial/\partial\zeta = 0$ are employed. Care is taken to insure that the flowfield has attained an asymptotic two-dimensional state in the vicinity of the $\eta = 1$ and $\zeta = 1$ boundaries. In particular, this requires that the width of the computational domain in the z direction be sufficiently large so that the shock wave created by the wedge passes out the downstream ($\xi = 1$) boundary.

Numerical Algorithm

The numerical algorithm is a hybrid explicit-implicit technique which combines the explicit finite difference algorithm of MacCormack[16,17] with an implicit algorithm for the viscous sublayer and transition wall region of the turbulent boundary layers (denoted the "computational sublayer"). The present 3-D algorithm is an extension of the technique developed previously for the 2-D Navier-Stokes equations by the present author.[18-20] The motivation for the development of the hybrid algorithm is to improve computational efficiency. Specifically, the exceedingly fine mesh spacing needed to resolve the viscous sublayer would impose a stringent restriction on the allowable time step for MacCormack's explicit method. In order to overcome this con-

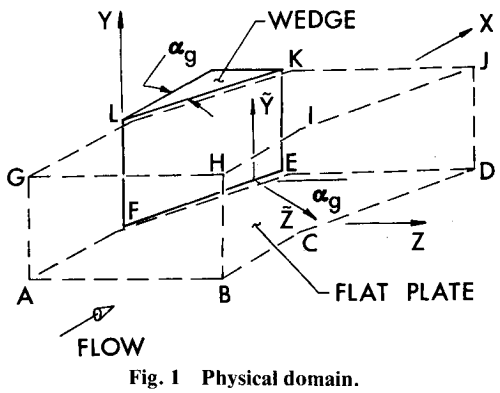

Fig. 1 Physical domain.

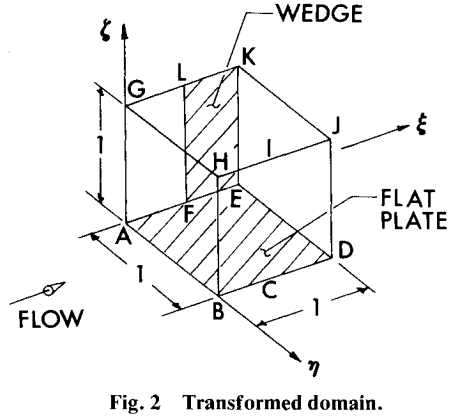

Fig. 2 Transformed domain.

straint, a separate implicit treatment of the computational sublayer is employed. MacCormack's explicit method is utilized for the region outside the computational sublayer, where the larger grid spacing allows a greater time step and, hence, improved computational efficiency.

On the set of grid points *outside* the computational sublayer (Fig. 4), denoted the "ordinary points," the Navier-Stokes equations are solved using MacCormack's second-order accurate explicit method.[16,17] The procedure consists of repetitive application of a finite difference operator $\mathcal{L}(\Delta t)$ which is a symmetric sequence of time-split, one-dimensional, finite difference operators[17] $\mathcal{L}_\xi(\Delta t_\xi)$, $\mathcal{L}_\eta(\Delta t_\eta)$, and $\mathcal{L}_\zeta(\Delta t_\zeta)$ given by

$$\mathcal{L}(\Delta t) = \mathcal{L}_\zeta^m(\Delta t/2m)\,\mathcal{L}_\eta^m(\Delta t/2m)\,\mathcal{L}_\xi(\Delta t) \times \mathcal{L}_\eta^m(\Delta t/2m)\,\mathcal{L}_\zeta^m(\Delta t/2m) \tag{5}$$

where the exponent m indicates the operator is applied m times. The time step Δt and exponent m are determined by the requirement of numerical stability of each operator[17] throughout the domain of ordinary mesh points. The fourth-order pressure damping term of MacCormack[17] is employed with a damping coefficient equal to -0.5.

On a separate set of grid points inside the computational sublayer, denoted the "sublayer points," the limiting form of the Navier-Stokes equations is employed. Consider a *local* Cartesian coordinate system (x', y', z') with the z' axis normal to the local tangent plane on the surface as illustrated in Fig. 4. The local Cartesian velocity components are denoted (u', v', w'). As z' approaches zero, the effects of streamwise convection (i.e., convection in the x'-y' plane) vanish due to the requirement of zero tangential velocity at the surface. Furthermore, as $z' \to 0$ the effects of diffusion of momentum and energy in the z' direction are substantially greater than those in the x'-y' plane, provided that the region of interest is not in the vicinity of a "corner" (i.e., a portion of the surface where one or both of the principal radii of curvature are small compared to the height of the computational sublayer region†). The governing equations in the computational sublayer are[26]

$$\frac{\partial \rho w'}{\partial z'} = 0 \tag{6}$$

$$\rho w' \frac{\partial u'}{\partial z'} = -\frac{\partial p}{\partial x'} + \frac{\partial}{\partial z'}\left[(\mu+\epsilon)\frac{\partial u'}{\partial z'}\right] \tag{7}$$

$$\rho w' \frac{\partial v'}{\partial z'} = -\frac{\partial p}{\partial y'} + \frac{\partial}{\partial z'}\left[(\mu+\epsilon)\frac{\partial v'}{\partial z'}\right] \tag{8}$$

$$\frac{\partial p}{\partial z'} = 0 \tag{9}$$

$$\rho w' \frac{\partial H}{\partial z'} = \frac{\partial}{\partial z'}\left[c_p\left(\frac{\mu}{Pr} + \frac{\epsilon}{Pr_t}\right)\frac{\partial T}{\partial z'}\right] + \frac{\partial}{\partial z'}\left\{(\mu+\epsilon)\frac{\partial}{\partial z'}\left[\frac{1}{2}(u'^2+v'^2)\right]\right\} \tag{10}$$

where $H = c_p T + \tfrac{1}{2}(u'^2+v'^2)$. The pressure gradient terms $\partial p/\partial x'$ and $\partial p/\partial y'$ are evaluated near the edge of the sublayer using the flowfield solution on the ordinary points, consistent with Eq. (9). The above equations represent the extension to three dimensions of the equations employed in previous study[29] and 2-D Navier-Stokes computations.[18-20] The temporal derivative terms are omitted since only the steady-state solution is desired. The computational sublayer equations are solved using the second-order accurate box scheme.[30] Based upon previous study,[18-20] the sublayer region is taken to be defined by $z'^+ \lesssim 60$, where $z'^+ = z' u_*/\nu_w$, with $u_* = (\tau_w/\rho_w)^{1/2}$. It shoud be emphasized that the height of the sublayer region corresponds to a small fraction of the height of the turbulent boundary layer (typically less than 5%).

In the vinicity of a corner, the limiting form of the governing equations differs from Eqs. (6-10) due to the presence of the two boundaries. Guided by asymptotic analysis for incompressible flows,[31] the governing equations to lowest order for a corner formed by two mutually orthogonal planes may be taken as

$$0 = -\frac{\partial p}{\partial x'} + \frac{\partial}{\partial y'}\left[(\mu+\epsilon)\frac{\partial u'}{\partial y'}\right] + \frac{\partial}{\partial z'}\left[(\mu+\epsilon)\frac{\partial u'}{\partial z'}\right] \tag{11}$$

$$\frac{\partial p}{\partial y'} = 0 \qquad \frac{\partial p}{\partial z'} = 0 \tag{12}$$

$$0 = \frac{\partial}{\partial y'}\left[c_p\left(\frac{\mu}{Pr} + \frac{\epsilon}{Pr_t}\right)\frac{\partial T}{\partial y'} + (\mu+\epsilon)\frac{\partial}{\partial y'}(\tfrac{1}{2}u'^2)\right] + \frac{\partial}{\partial z'}\left[c_p\left(\frac{\mu}{Pr} + \frac{\epsilon}{Pr_t}\right)\frac{\partial T}{\partial z'} + (\mu+\epsilon)\frac{\partial}{\partial z'}(\tfrac{1}{2}u'^2)\right] \tag{13}$$

where u' is the velocity component in the direction of the line of intersection FE of the two surface planes (Fig. 1). The term $\partial p/\partial x'$ is evaluated near the edge of the sublayer using the flowfield solution on the ordinary points, consistent with Eq. (12). The temporal derivative terms have been omitted since only the steady-state solution is desired. The corner sublayer equations are expressed in finite difference form using second-order accurate central differences and solved using Newton iteration. Again, it is emphasized that the physical size of the corner sublayer region represents a small fraction of the local boundary-layer thickness.

The solution procedure consists of integration of the Navier-Stokes equations on the ordinary grid points from time t to time $t+\Delta t$ using MacCormack's method, followed by solution of Eqs. (6-13) in the sublayer regions, with the flowfield solutions on the sublayer and ordinary grids matched at the interface. The procedure is continued until a steady-state solution is obtained.

The hybrid algorithm has been vectorized on the CDC CYBER 203 computer using the SL/1 programming language developed at NASA Langley. The data management architecture of Smith and Pitts,[32,33] based on an interleaved data base,[34] is employed. The improvement in efficiency obtained through vectorization of MacCormack's explicit algorithm can be evaluated in terms of the operator processing time (OPT), which is defined as the effective time required to apply one operator (e.g., $\mathcal{L}_\xi$, $\mathcal{L}_\eta$, or $\mathcal{L}_\zeta$) to one mesh point. From Eq. (5), the total CPU time for the ordinary grid is $N_t \times N_m \times N_0 \times \text{OPT}$, where N_t is the number of time steps, N_m the number of mesh points, and N_0 the number of operators in Eq. (5). For the present code on the CYBER 203, $\text{OPT} = 1.26 \times 10^{-5}$ s, which is a factor of 111 times faster[18-20] than on the CYBER 74, in agreement with previous studies.[32,35,36]

The accuracy of the hybrid algorithm for two-dimensional flows previously has been demonstrated[18-20] for a variety of cases including shock wave/turbulent boundary-layer in-

†For example, in the vicinity of a 90-deg corner (where the principal radii of curvature are zero and infinity), the diffusion effects become essentially two dimensional as the corner is approached.

teraction with flow separation and several configurations of a simulated 2-D high-speed inlet. The accuracy of the hybrid algorithm was investigated for three-dimensional flows for the specific configuration of supersonic turbulent flow in a 90-deg corner. The computed results using the hybrid algorithm were found to be in close agreement with a separate calculation employing MacCormack's explicit algorithm only.[26,37]

Results for 3-D Oblique Shock Wave/Turbulent Boundary-Layer Interaction

The flow geometry (Fig. 1) consists of a 90-deg corner formed by a flat plate and a wedge of angle α_g. A supersonic equilibrium turbulent boundary layer develops on the flat plate. An oblique shock, formed by the wedge, intersects the turbulent boundary layer on the flat plate, resulting in a 3-D turbulent interaction. This flowfield has been surveyed extensively by Oskam et al.[3,4,38,39] at Mach 3 for $\alpha_g \leq 14$ deg, and computations have been performed by Horstman and Hung[12] for $\alpha_g = 3.75$ and 9.75 deg using the algebraic turbulent eddy-viscosity model of Escudier.[40] In the present effort, computations were performed[26] using the Baldwin-Lomax turbulence model for $\alpha_g = 3.73$ and 9.72 deg at a freestream Mach number $M_\infty = 2.94$, total pressure $p_{t_\infty} = 689.7$ kPa, and total temperature $T_{t_\infty} = 255.6$ K. The flat-plate temperature is 280.6 K, which is 17% above the adiabatic recovery temperature. The wedge temperature is 244.4 and 252.8 K for $\alpha_g = 3.73$ and 9.72 deg, respectively. The results for the $\alpha_g = 9.72$ deg case are presented herein, with emphasis on evaluation of the efficiency of the hybrid algorithm and the accuracy of the Baldwin-Lomax turbulence model. The reader is referred to Refs. 3, 4, 9, 12, 38, and 39 for a detailed description of the flow structure.

Details of Computation

The upstream boundary-layer profile, which provides the upstream boundary condition on $\xi = 0$, is obtained by computing the development of a flat-plate boundary layer to a point where the computed momentum thickness is equal to the experimental value $\theta_\infty = 0.063$ cm. At this station, the computed and measured displacement thicknesses δ^*_∞ are 0.335 and 0.41 cm, respectively, and the computed and measured skin friction coefficients c_f are 1.08 and 1.19×10^{-3}, respectively. The value of c_f predicted by the Van Driest II theory[41] is 1.148×10^{-3}. The computed and measured values of the boundary-layer thickness agree ($\delta_\infty = 1.37$ cm), and the velocity profiles are in close agreement with the laws of the wall and wake.[42] The overall agreement between the computed and measured upstream profiles is comparable to that achieved by Horstman and Hung.[12]

The numerical grid consists of a set of streamwise planes spaced uniformly by an amount Δx in the x direction. Within each plane, the grid points were distributed in the y and z directions using a combination of geometric stretching near the flat plate and wedge and uniform spacing outside the boundary layers.[26] In evaluating the resolution afforded by the numerical grid, attention was focused on the capability of the grid to resolve pertinent flow features in four main areas; namely, 1) the boundary layers in the direction normal to the walls, 2) the boundary layers in the cross-stream direction (e.g., in the y direction on the wedge), 3) the inviscid regions of the flowfield in each streamwise plane, and 4) the flowfield in the streamwise x direction. It was judged that reasonably precise criteria existed only for item 1, and therefore two separate computations were performed (Table 1) to examine the remaining three. With regard to item 1, the resolution of the boundary layers in the direction normal to the walls was judged satisfactory for both cases, since the distance (in wall units) of the first row of grid points adjacent to the boundaries $\Delta z_2'^+$ is less than 3.2 for all cases (Table 2), and the typical number of grid points within the boundary layers on the wedge and flat plate is 17 and 20, respectively.[18-20] Regarding item 2, the mesh spacing in the cross-stream direction consists of a combination of geometric stretching and uniform spacing, with the maximum values (i.e., $\Delta y_\infty/\delta_\infty$ and $\Delta z_\infty/\delta_\infty$) indicated in Table 2. The maximum values of $\Delta z/\delta_\infty$ are 0.49 and 0.77 for grids 1 and 2, thus providing an opportunity for evaluation. With regard to item 3, the inviscid regions of the flow are covered primarily by the uniformly spaced grid, and the variation in $\Delta z_\infty/\delta_\infty$ between grids 1 and 2 permits an approximate evaluation of resolution of the inviscid regions. With regard to item 4, the streamwise mesh spacing $\Delta x/\delta_\infty$ is 0.46 and 0.93 for grids 1 and 2, and thus provides an opportunity for examination of the adequacy of the streamwise resolution.

The initial condition for all cases was obtained by extending the upstream profile to all stations. Each case was judged converged to steady state after a physical time of approximately $3.4t_c$, where t_c is the time required for a fluid parcel to travel from the upstream to the downstream end of the mesh in the inviscid region.[26]

The computer time required using the hybrid algorithm on the CYBER 203 is listed in Table 3. It should be emphasized that the numerical code has been developed for arbitrary flow regions, and incorporates a general three-dimensional steady coordinate transformation with the full nine coordinate transformation derivatives. The code was not specially modified to take advantage of the simplified geometry of the corner flow (for which only four coordinate transformation derivatives are nonzero), and the computer time, therefore, is representative of the resources required for the computation of a similar 3-D flowfield with a more general geometry.

Table 1 Details of mesh distribution

α_g	N_x[a]	N_y[a]	N_z[a]	NSL[b]
9.72 deg				
Grid 1	48	27	46	7
Grid 2	25	27	37	7

[a] N_x, N_y, N_z are the number of *ordinary* mesh points in x, y, and z directions.
[b] NSL is the number of mesh points in z' direction in the *sublayer*.

Table 2 Details of mesh resolution

	Wedge		Flat plate				
α_g	$\max\Delta z_2'^{+}$[a]	NBL[b]	$\max\Delta z_2'^{+}$[b]	NBL[b]	$\frac{\Delta x}{\delta_\infty}$[c]	$\frac{\Delta y_\infty}{\delta_\infty}$[d]	$\frac{\Delta z_\infty}{\delta_\infty}$[d]
9.72 deg							
Grid 1	3.19	17	2.65	20	0.46	0.58	0.49
Grid 2	3.05	17	3.20	20	0.93	0.58	0.77

[a] $\max\Delta z_2'^{+}$ = maximum value of $\Delta z_2'^{+}$, where $\Delta z_2'^{+} = \Delta z_2' u_*/\nu_w$, where $\Delta z_2'$ is the distance of the first row of sublayer points from the boundary.
[b] NBL = total number of points in boundary layer. For the wedge, NBL is evaluated at point K in Fig. 1. For the flat plate, NBL is the typical number of points in the boundary layer.
[c] Δx = mesh spacing in the x direction.
[d] Δy_∞, Δz_∞ = ordinary mesh spacing in the y and z directions in the region of the uniform grid.

The hybrid algorithm, vectorized on the CYBER 203, is significantly faster than a vectorized version of MacCormack's explicit algorithm alone on the same computer. The estimated computer time for each case using MacCormack's algorithm only according to Eq. (5) (with an $OPT = 1.26 \times 10^{-5}$), and the same grid distribution as used for the hybrid calculations, is shown in Table 3. It is evident that the hybrid algorithm is a factor of 16 to 21 times faster. In comparison to a vectorized, non-time-split version of MacCormack's explicit algorithm (assuming an $OPT = 1.3 \times 10^{-5}$ for the entire unsplit operator), the hybrid code is a factor of 8 to 10 times faster. The 2-D version of the hybrid algorithm[18-20] has been compared with the implicit method of Beam and Warming[43] on a scalar processing[27] computer (IBM 370/168) for a 2-D Navier-Stokes calculation of a Mach 3 adiabatic flat-plate turbulent boundary layer using the same number of grid points, grid resolution, initial conditions, and total physical time of computation. The 2-D hybrid method demonstrated approximately the same efficiency as the 2-D Beam-Warming code (the computer time was 12% more for the hybrid method). Although a 3-D Beam-Warming Navier-Stokes algorithm has been executed on the CYBER 203, this particular code[44] was not vectorized and consequently does not reflect the maximum efficiency obtainable for the Beam-Warming algorithm on the CYBER 203. A comparison of this code with the present vectorized hybrid method, therefore, is inappropriate.

Results for $\alpha_g = 9.72$ deg

The computed and experimental surface pressure on the flat plate at $x = 14.1\delta_\infty$ is displayed in Fig. 5, where z_g is the distance from the wedge surface, the subscript ∞ denotes upstream freestream conditions, and the arrow indicates the spanwise location of the shock at this station. The calculated profiles for grid 1 ($\Delta x/\delta_\infty = 0.46$) and grid 2 ($\Delta x/\delta_\infty = 0.93$) are in excellent agreement, with a maximum difference of 1%. The computed and measured pressures are in close agreement with a maximum difference of less than 5% (the experimental uncertainty[38] is $\pm 2\%$ of p_∞). The corner pressure agrees to within 3.6%. Additional comparison of profiles $x/\delta_\infty = 8.46$, 9.4, 10.4, 13.1, 14.9, 15.9, and 16.8 (not shown) indicates similar agreement. First, the maximum difference in computed profiles for grids 1 and 2 is 1%. Second, the maximum difference between the calculated and experimental profiles at these stations is 3.3, 5.4, 4.0, 5.0, 6.0, 7.0, and 4.0%, respectively. Third, the maximum overall difference between computed and experimental corner pressure is 4.0%. The computed profile of Horstman and Hung[12] at $x = 14.1\delta_\infty$ shows similar close agreement with experiment.

In Fig. 6, the computed and experimental normalized heat-transfer coefficient on the flat plate at $x = 14.1\delta_\infty$ is shown, where $c_h = q_w/\rho_\infty U_\infty c_p (T_w - T_{aw})$, q_w is the wall heat flux, T_w the wall temperature, and T_{aw} the adiabatic wall temperature evaluated by $T_{aw} = T_\infty + r(T_{t_\infty} - T_\infty)$, where $r = 0.89$ is the recovery factor.[38] The corresponding experimental and calculated c_{h_∞} (7.1 and 6.56×10^{-4}, respectively) are employed. Although these values differ by 8.2%, this discrepancy is within the experimental uncertainty[38] ($\pm 15\%$ of c_{h_∞}). The computed results for the two grids are in good agreement, except for the more pronounced "kink" in c_h for grid 1 at $z_g/\delta_\infty = 0.2$. This "kink" is attributable to the Baldwin-Lomax model.[26] The computed peak c_h/c_{h_∞} at $z_g/\delta_\infty = 0.2$ is 7.2% below the experiment, and thus within the uncertainty of the measurements. Comparison with three additional profiles (not shown) at $x/\delta_\infty = 8.5$, 9.4, and 13.1 displays similar agreement. First, the difference in peak c_h for the two grids is less than 5.5% at all stations. Second, the difference in the peak computed c_h/c_{h_∞} (using grid 1) and experiment is 3.8, 5.5, and 8.0%, respectively, at the three stations. It is noted[39] that the peak heat transfer is approximately 50% higher than the value predicted by the empirical correlation $q_{w_{max}}/q_{w_\infty} = (p_{max}/p_\infty)^{0.85}$ which has been developed for 2-D turbulent interactions.

Two profiles of the computed and experimental yaw angle $\alpha = \tan^{-1}(w/u)$ at $x = 14.1\delta_\infty$ are presented in Fig. 7. The spanwise locations are $z_g/\delta_\infty = 0.47$ and 4.2. At this station, the shock is located at $z_g/\delta_\infty = 5.03$. The computed profiles using grids 1 and 2 are in excellent agreement, with only a slight difference in the inviscid region at $z_g/\delta_\infty = 4.2$, which is less than 2 deg. The calculated profile at $z_g/\delta_\infty = 0.47$ is in excellent agreement with experiment (the experimental uncertainty[38] is ± 0.1 deg). The comparison at $z_g/\delta_\infty = 4.2$ displays good agreement, with a maximum difference of 4.8 deg. The rapid increase of yaw angle within the boundary layer is evident, with values reaching 36 deg close to the flat plate. Comparison with 18 additional profiles[38] (not shown)

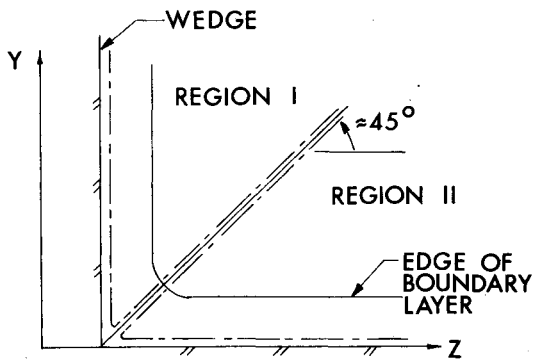

Fig. 3 Definition of regions for turbulent eddy viscosity.

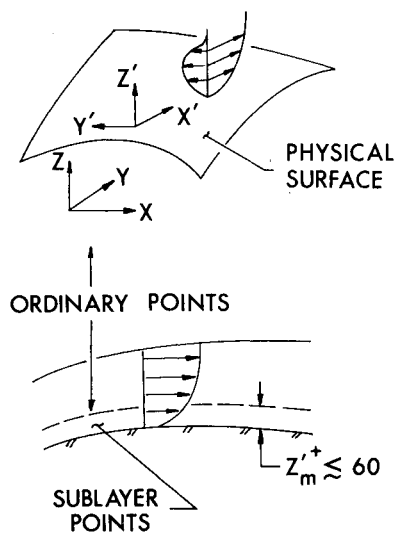

Fig. 4 Geometry of hybrid technique.

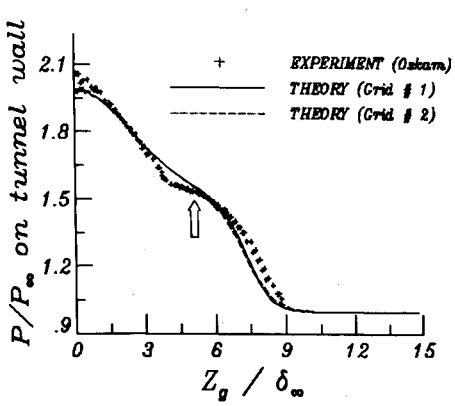

Fig. 5 Surface pressure on flat plate at $x/\delta_\infty = 14.1$.

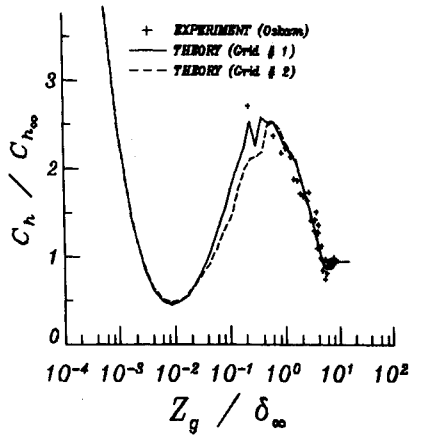

Fig. 6 Heat-transfer coefficient on flat plate at $x/\delta_\infty = 14.1$.

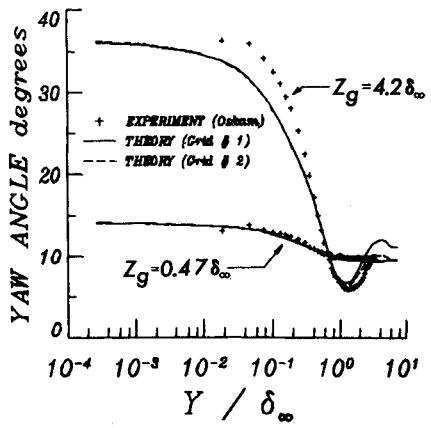

Fig. 7 Yaw angle profiles at $x/\delta_\infty = 14.1$.

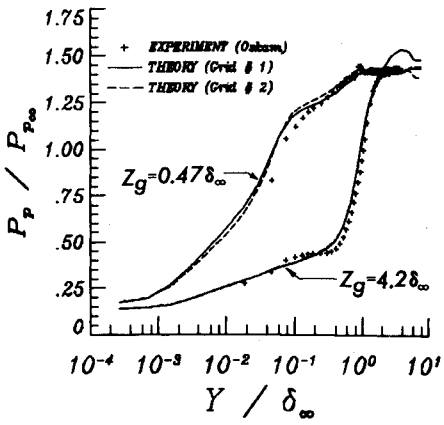

Fig. 8 Pitot pressure profiles at $x/\delta_\infty = 14.1$.

Table 3 Computer time

α_g	Total No. grid points	Computer time on CYBER 203, h: Hybrid algorithm	Computer time on CYBER 203, h: Vectorized MacCormack explicit [a] algorithm [(Eq. (5)]
3.73 deg 9.72 deg	28,230	1.28	27.1
Grid 1	79,727	5.35	88.9
Grid 2	34,232	2.20	35.3

[a] Estimated.

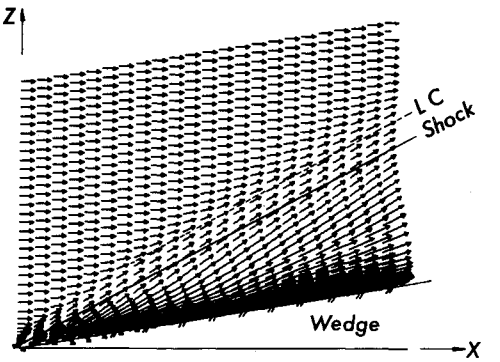

Fig. 9 Shear stress on flat plate.

confirm the above findings. First, the computed profiles using the two grids are in excellent agreement. The maximum difference within the boundary layer is less than 1 deg, and the maximum difference outside the boundary layer is less than 2 deg. Second, the computed profiles are in good agreement with experiment. Specifically, comparison of profiles with $0 < z_g/z_{gs}(x) < 0.7$ [where $z_{gs}(x)$ is the shock location] indicates a maximum difference of less than 3 deg, although the yaw angle reaches values as large as 35 deg. For $0.7 < z_g/z_{gs}(s) < 1.45$ (the spanwise limit of the measurements), the maximum difference is less than 6 deg.

In Fig. 8, two profiles of the calculated and measured pitot pressure p_p at $x = 14.1\delta_\infty$ are shown. The spanwise locations are the same as for Fig. 7. The computed profiles using the two grids are in close agreement within the boundary layer, with a maximum difference of 4.7% at $z_g/\delta_\infty = 0.47$ and less than 1% at $z_g/\delta_\infty = 4.2$. The computed profiles display a maximum disagreement of 6.8% in the inviscid region at $z_g/\delta_\infty = 4.2$, which is associated with the proximity of this location to the shock $[z_{gs}(x)/\delta_\infty = 5.03]$ and the shock-capturing nature of the algorithm. The calculated profiles are observed to be in good agreement with experiment. At $z_g/\delta_\infty = 0.47$, the maximum difference between the calculated and measured profiles is less than 5% of p_{p_∞} everywhere (except for the data point closest to the plate at $y = 0.025$ cm). The experimental uncertainty[38] is $\pm 1\%$ of p_{p_∞}. At $z_g/\delta_\infty = 4.2$, the maximum difference is less than 9.0% of p_{p_∞}. Comparison with 18 additional profiles[18] (not shown) shows similar characteristics. First, the computed profiles using the two grids are in excellent agreement. The maximum difference within the boundary layer is less than 1%, except for three profiles (at different x) close to the corner (z_g/δ_∞ typically equal to 0.1) for which the maximum difference is less than 5.0%. Second, the computed profiles are in reasonable agreement with experiment. The maximum difference between the calculated and experimental results is less than 10% for 15 of the 18 profiles, and less than 15.6% for the remaining profiles.

In Fig. 9 the direction and magnitude of the surface shear stress on the flat plate is shown. The vectors also indicate the direction of the limiting streamlines.[45] The flow geometry is reflected in the x-y plane for comparison with the experimental oil flow pattern (Fig. 10). A line of coalescence ("three-dimensional separation line"[5]; also, see Ref. 46) forms upstream of the shock location in Fig. 10. The computed coalescence line, which represents an asymptote of the surface shear stress, is in good agreement with the experimental oil film coalescence line. In particular, at $x/\delta_\infty = 10.0$ the normal distance of the coalescence line from the shock line is approximately $1.2\delta_\infty$ in the experiment and $1.3\delta_\infty$ in the calculation. Computations by Horstman and Hung[12] of the flow streamlines for this and other cases

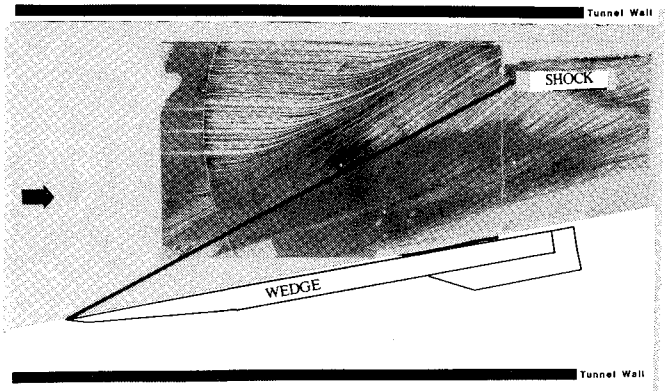

Fig. 10 Experimental oil film pattern.

exhibiting coalescence of the surface shear stress have shown a significant lifting of the fluid in the vicinity of the line of coalescence.

Conclusions

An accurate and efficient hybrid numerical algorithm has been developed for the three-dimensional mean compressible Navier-Stokes equations. The algebraic turbulent eddy-viscosity model of Baldwin and Lomax is employed. A general body-fitted coordinate transformation is incorporated to facilitate treatment of arbitrary flow regions. The hybrid algorithm combines the explicit finite difference method of MacCormack with an implicit treatment of the viscous sublayer and transition wall region of the turbulent boundary layers, and represents the extension to three dimensions of the hybrid algorithm developed and tested for two-dimensional flows. The hybrid algorithm has been vectorized on the CYBER 203 computer using the SL/1 vector programming language developed at NASA Langley Research Center. The accuracy of the hybrid algorithm for three-dimensional flows was validated by comparison with a separate computation using MacCormack's method alone for the case of supersonic turbulent flow in a 90-deg corner formed by two flat plates.

The hybrid algorithm was applied to the interaction of an oblique shock wave, formed by a wedge of angle α_g, with a turbulent boundary layer in three dimensions at Mach 3. Results are presented for $\alpha_g = 9.72$ deg for two separate numerical grids, which differed principally in the streamwise grid spacing ($\Delta x/\delta_\infty = 0.46$ and 0.93). The agreement between the computed profiles is very good. The agreement between the calculated and experimental profiles of surface pressure and heat transfer, yaw angle, and pitot pressure is good. The method of Baldwin and Lomax for determination of the length and velocity scales for the outer turbulent eddy viscosity was found to be deficient in certain regions of the interaction, and a modified method was employed. The hybrid algorithm provides a substantial improvement in computational efficiency. The computer time for the two computations is an approximate *factor* of 16-21 times less than would be required using a vectorized version of MacCormack's time-split algorithm on the CYBER 203.

Acknowledgments

This research is sponsored by the Air Force Flight Dynamics Laboratory/Air Force Wright Aeronautical Laboratories, the Air Force Office of Scientific Research, and NASA Langley Research Center under AFOSR Grants 82-0040 and 80-0072, monitored by Dr. J. Wilson and J. Mace. The author acknowledges helpful discussions with S. Bogdonoff, D. Dolling, C. Horstman, J. Pitts, G. Settles, and R. Smith.

References

[1]Law, C. H., "Three-Dimensional Shock Wave-Turbulent Boundary Layer Interactions at Mach 6, "Aerospace Research Laboratories, Wright-Patterson AFB, Ohio, ARL-TR-75-0191, June 1975.

[2]Freeman, L. M. and Korkegi, R. H., "Experiments on the Interaction with a Turbulent Boundary Layer of a Skewed Shock-Wave of Variable Strength at Mach 2.5," Aerospace Research Laboratories, Wright-Patterson AFB, Ohio, ARL-TR-0182, June 1975.

[3]Oskam, B., Vas., I. E., and Bogdonoff, S. M., "Mach 3 Oblique Shock Wave/Turbulent Boundary Layer Interactions in Three Dimensions," AIAA Paper 76-336, 1976.

[4]Oskam, B., Vas, I.E., and Bogdonoff, S.M., "An Experimental Study of Three-Dimensional Flow Fields in an Axial Corner at Mach 3," AIAA Paper 77-689, 1977.

[5]Peake, D. J., "Three-Dimensional Swept Shock/Turbulent Boundary Layer Separations with Control by Air Injection," National Research Council, Canada, Aeronautic Rept. LR-592, July 1976.

[6]Settles, G. S., Perkins, J. J., and Bogdonoff, S. M., "Investigation of Three-Dimensional Shock/Boundary-Layer Interactions at Swept Compression Corners," *AIAA Journal,* Vol. 18, July 1980, pp. 779-785.

[7]Dolling, D. S., Cosad, C. D., and Bogdonoff, S. M., "An Examination of Blunt Fin- Induced Shock Wave Turbulent Boundary Layer Interactions," AIAA Paper 79-0068, 1979.

[8]Settles, G. S. and Bogdonoff, S. M., "Scaling of 2-D and 3-D Shock/Turbulent Boundary Layer Interactions in Compression Corners," *AIAA Journal,* Vol. 20, June 1982, pp. 782-789.

[9]Dolling, D. S. and Bogdonoff, S. M., "Upstream Influence Scaling of Sharp Fin-Induced Shock Wave Turbulent Boundary Layer Interactions," AIAA Paper 81- 0336, 1981.

[10]Hung, C. M. and MacCormack, R. W., "Numerical Solution of Three-Dimensional Shock Wave and Turbulent Boundary Layer Interaction," *AIAA Journal*, Vol. 16, Oct. 1978, pp. 1090-1096.

[11]Shang, J. S., Hankey, W. L., and Petty, J. S., "Three-Dimensional Supersonic Interacting Turbulent Flow Along a Corner," *AIAA Journal*, Vol. 17, July 1979, pp. 706-713.

[12]Horstman, C. C. and Hung, C. M., "Computation of Three-Dimensional Turbulent Separated Flows at Supersonic Speeds," AIAA Paper 79-0002, 1979.

[13]Hung, C. M. and Chaussee, D. S., "Computation of Supersonic Turbulent Flows Over an Inclined Ogive-Cylinder Flare," *AIAA Journal*, Vol. 19, Sept. 1981, pp. 1139-1144.

[14]Hung, C. M., "Impingement of an Oblique Shock Wave on a Cylinder, "AIAA Paper 82-0025, 1982.

[15]Baldwin, B. S. and Lomax, M., "Thin Layer Approximation and Algebraic Model for Separated Turbulent Flows," AIAA Paper 78-257, 1978.

[16]MacCormack, R. W., "Numerical Solution of the Interaction of a Shock Wave with a Laminar Boundary Layer," *Lecture Notes in Physics,* Vol. 8, 1971, pp. 151-163.

[17]Baldwin, B. S. and MacCormack, R. W., "A Numerical Method for Solving the Navier-Stokes Equations with Application to Shock-Boundary Layer Interactions," AIAA Paper 75-1, 1975.

[18]Knight, D. D., "Improved Calculation of High Speed Inlet Flows: Part I. Numerical Algorithm," *AIAA Journal,* Vol. 19, Jan. 1981, pp. 34-41.

[19]Knight, D. D., "Improved Calculation of High Speed Inlet Flows: Part II. Results," *AIAA Journal*, Vol. 19, Feb. 1981, pp. 172-179.

[20]Knight, D. D., "Calculation of High-Speed Inlet Flows Using the Navier-Stokes Equations," *Journal of Aircraft,* Vol. 18, Sept. 1981, pp. 748-754.

[21]Thompson, J. and Warsi, Z., "Boundary Fitted Coordinate Systems for Numerical Solution of Partial Differential Equations—A Review," *Journal of Computational Physics,* Vol. 47, 1982, pp. 1-108.

[22]Rubesin, M. and Rose, W., "The Turbulent Mean-Flow, Reynolds-Stress and Heat-Flux Equations in Mass Averaged Dependent Variables," NASA TMX-62248, March 1973.

[23]Pulliam, T. and Steger, J., "Implicit Finite-Difference Simulations of Three-Dimensional Compressible Flow," *AIAA Journal,* Vol. 18, Feb. 1980, pp. 159-167.

[24]Buleev, N., "Theoretical Model of the Mechanism of Turbulent Exchange in Fluid Flows," Atomic Energy Research Establishment, Hartwell, England, AERE Translation 957, 1963.

[25]Gessner, F. and Po, J., "A Reynolds Stress for Turbulent Corner Flows-Part II: Comparisons Between Theory and Experiments," *Journal of Fluid Engineering, Transactions of ASME,* Vol. 98, Ser. 1, No. 2, June 1976, pp. 269-277.

[26]Knight, D., "A Hybrid Explicit-Implicit Numerical Algorithm for the Three-Dimensional Compressible Navier-Stokes Equations," AIAA Paper 83-0223, 1983.

[27] Visbal, M. and Knight, D., "Evaluation of the Baldwin-Lomax Turbulence Model for Two-Dimensional Shock Wave Boundary Layer Interactions," AIAA Paper 83-1697, 1983.

[28] Degani, D. and Schiff, L., "Computation of Supersonic Viscous Flows Around Pointed Bodies at Large Incidence," AIAA Paper 83-0034, 1983.

[29] Cebeci, T., "Calculations of Compressible Turbulent Boundary Layers with Heat and Mass Transfer," *AIAA Journal,* Vol. 9, June 1971, pp. 1091-1097.

[30] Keller, H., "Accurate Difference Methods for Nonlinear Two-Point Boundary Value Problems," *SIAM Journal of Numerical Analysis,* Vol. 11, April 1974, pp. 305-320.

[31] Rubin, S., "Incompressible Flow Along a Corner," *Journal of Fluid Mechanics,* Vol. 26, 1966, pp. 97-110.

[32] Smith, R.E., "Numerical Solution of the Navier-Stokes Equations for a Family of Three-Dimensional Geometries," AIAA Paper 80-1349, 1980.

[33] Smith, R. E. and Pitts, J., "The Solution of the Three-Dimensional Viscous-Compressible Navier-Stokes Equations on a Vector Computer," *Advances in Computer Methods for Partial Differential Equations, Proceedings of the Third IMACS Symposium,* Rutgers University, New Brunswick, N.J., 1979, pp. 245-252.

[34] Lambiotte, J., "Effect of Virtual Memory on Efficient Solution of Two Model Problems," NASA TMX 3512, July 1977.

[35] Shang, J., Buning, P., Hankey, W., and Wirth, M., "The Performance of a Vectorized 3-D Navier-Stokes Code on the CRAY-1 Computer," *AIAA Journal,* Vol. 18, Sept. 1980, pp. 1073-1079.

[36] Kumar, A., "Three-Dimensional Inviscid Analysis of the Scramjet Inlet Flowfield," AIAA Paper 82-0060, 1982.

[37] Knight, D., "A Three-Dimensional Navier-Stokes Code for High Speed Inlets Using the CYBER 203 Computer," Dept. of Mechanical and Aeronautical Engineering, Rutgers University, New Brunswick, N.J., Rept. RU-TR-156-MAE-F, Feb. 1982.

[38] Oskam, B., Vas, I., and Bogdonoff, S., "Oblique Shock Wave/Turbulent Boundary Layer Interactions in Three Dimensions at Mach 3," Air Force Flight Dynamics Laboratory, Wright-Patterson AFB, Ohio, AFFDL-TR-76-48, Pt. I, June 1976; Pt. II, March 1978.

[39] Oskam, B., "Three-Dimensional Flow Fields Generated by the Interaction of a Swept Shock Wave with a Turbulent Boundary Layer," Princeton Gas Dynamics Lab, Princeton, N.J., Rept. 1313, Dec. 1976.

[40] Escudier, M., "The Distribution of the Mixing Length in Turbulent Flows Near Walls," Mechanical Engineering Dept., Imperial College, London, Rept. TWF/TN/1, 1965.

[41] Hopkins, E. and Inouye, M., "An Evaluation of Theories for Predicting Turbulent Skin Friction and Heat Transfer on Flat Plates at Supersonic and Hypersonic Mach Numbers," *AIAA Journal,* Vol. 9, June 1971, pp. 993-1003.

[42] Sun, C-C. and Childs, M., "Wall-Wake Velocity Profile for Compressible Nonadiabatic Flows," *AIAA Journal,* Vol. 14, June 1976, pp. 820-822.

[43] Beam, R. and Warming, R., "An Implicit Factored Scheme for the Compressible Navier-Stokes Equations," *AIAA Journal,* Vol. 16, April 1978, pp. 393-402.

[44] Swanson, R., "Navier-Stokes Solutions for Nonaxisymmetric Nozzle Flows," AIAA Paper 81-1217, 1981.

[45] Rosenhead, L., ed., *Laminar Boundary Layers,* Oxford, England, 1963.

[46] Kubota, H. and Stollery, J., "An Experimental Study of the Interaction Between a Glancing Shock Wave and a Turbulent Boundary Layer," *Journal of Fluid Mechanics,* Vol. 116, March 1982, pp. 431-458.